SCIEPublish

Article

Photocatalytic CO_2 Fixation into Formate under Visible Light by the Photo-Enzyme Hybrid of Gold Nanocapsules and Formate Dehydrogenase

Yaoqiang Wang [1,2], Ming Gong [2], Huawen Wang [2], Gang Xiao [2,*], Haijia Su [2,*] and Jianmin Xing [1]

[1] CAS Key Laboratory of Green Process and Engineering & State Key Laboratory of Biochemical Engineering, Institute of Process Engineering, Chinese Academy of Sciences, Beijing 100190, China; wangyq122@foxmail.com (Y.W.); jmxing@ipe.ac.cn (J.X.)

[2] Beijing Advanced Innovation Center for Soft Matter Science and Engineering (BAIC-SM), College of Life Science and Technology, Beijing University of Chemical Technology, Beijing 100029, China; 304263715@qq.com (M.G.); 2582043237@qq.com (H.W.)

* Corresponding author. E-mail: sewicxiao@hotmail.com (G.X.); suhj@mail.buct.edu.cn (H.S.)

Received: 4 November 2024; Accepted: 25 November 2024; Available online: 27 November 2024

ABSTRACT: The photo-enzyme hybrid system presents a promising approach for the selective conversion of CO_2 into valuable chemicals. However, its high dependence on the expensive coenzyme nicotinamide adenine dinucleotide reduced form (NADH), coupled with the need for external electron mediators and highly active photocatalysts, limits its widespread application. Here, we developed a gold nanocapsule—formate dehydrogenase (FDH) hybrid system for in situ NADH regeneration to facilitate the light-driven conversion of CO_2 to formate. The results demonstrated that gold nanocapsules (Au NCPs), in conjunction with triethanolamine (TEOA), protected 83.67% of NADH from photodegradation. Under light-driven conditions with TEOA as the electron donor and without external electron mediators, the Au NCPs catalyzed in situ NADH regeneration, achieving a regeneration yield of 22.65%. This process aided FDH in reducing CO_2 to formate, resulting in a production rate of 67.40 μmol/L/h. This research provides valuable insights for developing photo-enzyme hybrid systems that efficiently convert CO_2 without the need for external electron mediators.

Keywords: Photo-enzyme hybrid system; NADH regeneration; Gold nanocapsules; CO_2 reduction; Formate

1. Introduction

The excessive reliance on fossil fuels in current human activities has resulted in excessive carbon dioxide (CO_2) emissions, leading to a range of potential ecological, physical, and health impacts [1,2]. Therefore, efficient and green methods should be developed to achieve CO_2 recycling in order to address CO_2 pollution and attain the goal of carbon neutrality as soon as possible. In recent years, the use of dehydrogenase cascade catalysis to convert CO_2 into compounds like formate and methanol has been extensively studied [3,4]. The enzymatic conversion of CO_2 to formic acid is a crucial step in these cascade reactions [3,5]. However, the high cost of dehydrogenases and the stoichiometric consumption of cofactors make practical carbon fixation using dehydrogenases unfeasible [6]. Therefore, it is necessary to develop efficient enzyme immobilization and cofactor regeneration systems, coupling enzymatic CO_2 reduction with cofactor regeneration for efficient operation [7].

Mimicking natural photosynthesis and using unlimited renewable solar energy to produce chemical fuels and other synthetic energy from CO_2 is one of the most promising solutions for high-value CO_2 conversion [8,9]. This artificial photosynthesis employs photocatalysts to immobilize dehydrogenases, creating photo-enzyme hybrids. These systems can catalyze the conversion of CO_2 into high-value compounds under visible light, using photo-catalytically regenerated NAD(P)H as the "energy currency" for enzymatic catalysis [10]. This approach integrates the excellent light-absorption properties of photocatalysts with the high activity and selectivity of enzymes [11].

https://doi.org/10.70322/prp.2024.10011

However, due to the poor photostability and high cost of NADH, to achieve continuous photocatalytic CO_2 reduction through photo-enzyme hybrids, an efficient and straightforward method for NADH recycling is essential [12,13]. Although many efficient photocatalytic NADH regeneration methods have been developed, most of these methods rely on organic electron mediators ($[Cp^*Rh(bpy)H_2O]^{2+}$ and $[Cp^*RhCl_2]_2$) to transfer electrons [14,15]. However, these electron mediators are expensive and can inhibit each other with FDH, significantly reducing enzyme activity [16,17]. Therefore, developing NADH regeneration technology that does not rely on exogenous electron mediators is particularly important for the sustainability of photo-enzyme coupling for carbon fixation. Moreover, immobilizing photocatalysts and enzymes on a carrier to construct a photo-enzyme hybrid system can help improve enzyme stability and the potential for reuse [18]. However, the free radical toxicity of photocatalysts makes this photo-enzyme hybrid system less stable [19]. Utilizing photocatalysts directly as enzyme carriers can simplify the photo-enzyme hybrid system, reduce the spatial distance between the photocatalysts and enzymes, enhance photoelectron transfer efficiency, and, in turn, promote enzyme-catalyzed reactions. Therefore, the choice and design of photocatalysts (enzyme carriers) are crucial for constructing photo-enzyme hybrid systems. Research indicates that gold nanocages, which are hollow cage-like nanomaterials assembled from gold nanocapsules (Au NCPs) with full-spectrum absorption characteristics, exhibit high photocatalytic efficiency due to their electromagnetic field enhancement effect [20]. Their high biocompatibility and hollow structure suggest potential for serving as both photocatalysts and enzyme carriers.

In this study, we employed Au NCPs as both the photocatalysts and the carriers for formate dehydrogenase (FDH). Initially, we investigated the protective performance of Au NCPs towards NADH under illumination and optimized their photocatalytic activity for NADH regeneration without external electron mediators. Subsequently, we constructed a light-enzyme hybrid system using the Au NCPs and FDH, optimizing the conditions for CO_2 reduction within this hybrid system. This approach achieved efficient light-driven CO_2 reduction to formate using the Au NCPs-FDH hybrid system, providing a solid foundation for developing photo-enzyme coupling hybrid systems and advancing light-driven enzyme catalysis for efficient carbon fixation.

2. Materials and Methods

The schematic diagram of the preparation of gold nanoparticles, gold nanocapsules, and the immobilization of formate dehydrogenase (FDH) to construct the photo-enzyme hybrid system is shown in Scheme 1.

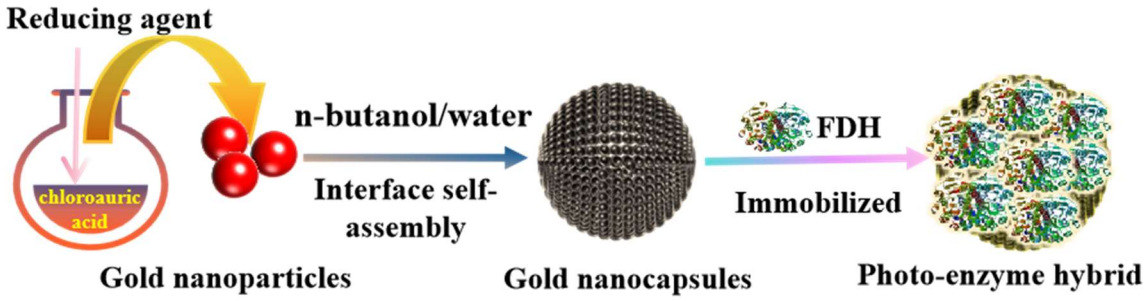

Scheme 1. Schematic diagram of the preparation of gold nanocapsules and the immobilization of FDH on the gold nanocapsules.

2.1. Preparation and Characterization of Gold Nanocapsules

Gold nanoparticles (Au NPs) preparation: Following the method reported by Li et al. [21], Au NPs were synthesized via the sodium citrate reduction of chloroauric acid. The pH of the reaction solution was adjusted to 2 using 2 M hydrochloric acid. The Au NPs were then precipitated by adding isopropanol in a 1:1 volume ratio with the reaction solution. The precipitated Au NPs were washed sequentially three times each with methanol and n-butanol. Finally, the Au NPs were resuspended in ultrapure water and concentrated to obtain a 20 wt% suspension.

Synthesis of gold nanocapsules (Au NCPs): Following previous reports [20], a suspension of Au NPs and n-butanol were mixed in various volume ratios to create two distinct phases with a clear oil-water interface. The aqueous phase was emulsified in n-butanol through vortex shaking for 60 s and ultrasonication for 5 min. The resulting emulsion, encapsulating the gold nano colloids, was left to stand for 12 h, allowing the gold particles to self-assemble into Au NCPs at the oil-water interface. The Au NCPs were then separated by centrifugation, washed sequentially three times with n-butanol and ethanol, freeze-dried for 24 h, and stored at 4 °C for future use.

The morphology and cavity structure of the Au NCPs were observed using a transmission electron microscope (JEOL JEM 2100F, Tokyo, Japan). In contrast, the external structure was observed using a scanning electron microscope (Hitachi SU8600 SEM, Tokyo, Japan). The UV-vis spectra of both Au NPs and Au NCPs were measured using a TECAN microplate reader.

2.2. Photocatalytic Regeneration of NADH by Au NCPs

Protective properties of Au NCPs against NADH under light: NADH is known to be less stable under light and acidic conditions [22]. The effects of the electron donor triethanolamine (TEOA) and Au NCPs on the stability of NADH under light were first tested. A 2 mL reaction system containing 0.50 mM NADH, Au NCPs (1.25 mg/mL), and TEOA (100 mM) was maintained at a controlled temperature of 30 °C and irradiated with 50 mW/cm^2 LED white light. Samples were taken at 0, 1, 2, 4, 6, and 8 h. The remaining concentration of NADH was calculated by measuring its absorbance at 340 nm [23] to evaluate the protective performance of the Au NCPs on NADH under light exposure.

Photocatalytic NADH Regeneration: The multichannel photocatalytic reaction system (WATTCAS) was used to conduct the photocatalytic NADH regeneration experiments. The photocatalytic system containing NAD^+ (0.50 mM), TEOA, and Au NCPs (1.25 mg/mL) was exposed to LED white light for a certain period. The supernatant was periodically sampled to measure the concentration of NADH, and the regeneration yield of NADH was calculated using Equation (1).

$$\text{Regeneration yield} = \frac{C_{\text{NADH}}}{C_{\text{NAD}^+}} \times 100\ (\%) \quad (1)$$

2.3. Immobilization of FDH on Au NCPs for the Photo-Enzymatic Hybrid System

The FDH (0.10 mg/mL) was mixed with Au NCPs (1.50 mg/mL) in a buffer solution (100 mM, pH = 7.40) and shaken the mixture at a set temperature for a certain period. The protein concentration in the supernatant was measured using the Bradford assay, and the immobilization yield of FDH was calculated (Equation (2)). The photo-enzyme hybrid system was centrifuged at 8000 rpm for 5 minutes, and the precipitate was collected and washed twice with a buffer solution. Then, freeze-dry the precipitate and store it at 4 °C for future use. The activity of FDH was assessed by measuring the initial reduction rates of formate catalyzed by both free FDH and the photo-enzyme hybrid [9]. The free FDH, sodium formate (1 mM), and NAD^+ (10 mM) were added to PBS and shaken at room temperature for 3 min, and the absorbance at 340 nm was measured to determine free enzyme activity. The immobilized enzyme activity was evaluated by replacing the free FDH with the photo-enzyme hybrid while maintaining all other conditions constant. The recovery of enzyme activity was calculated according to Equation (3).

$$\text{Immobilization yield} = \frac{C_0 - C}{C_0} \times 100\ (\%) \quad (2)$$

where C_0 is the initial concentration of FDH (μg/mL); C is the residual protein concentration in the supernatant after the immobilization reaction (μg/mL).

$$\text{Recovery of enzyme activity} = \frac{A_1}{A} \times 100\ (\%) \quad (3)$$

where A_1 and A are the absorbance at 340 nm of the immobilized and free FDH, respectively, after their reaction with the substrate.

2.4. Light-Driven Photo-Enzyme Hybrid System for Converting CO_2 to Formate

The reaction solution included NAD^+ (0.50 mM), free FDH or Au NCPs—FDH hybrid (0.50 mg/mL) sodium molybdate, and TEOA (300 mM) dispersed into 2 mL of PBS (100 mM, pH = 7.40), and the reaction proceeded at 30 °C. Before the reaction, the system was purged with CO_2 (99.99%) for 5 min, then sealed with 200 mL of CO_2 gas bag, and then the reaction was carried out under the irradiation of LED white light (150 mW/cm^2). The formate concentration in the supernatant was determined by high-performance liquid chromatography (Agilent, Santa Clara, CA, USA) with a UV detector.

3. Results and Discussion

3.1. Morphological Structure and Light Absorption Properties of Gold Nanocapsules

Figure 1a shows the TEM image of the gold nanocapsules (Au NCPs), which were self-assembled from Au nanoparticles (Au NPs). The Au NCPs are presented as spherical structures, with a small number of Au nanoparticles at their edges, having an average particle size of 13.06 ± 2.49 nm (Figure 1b,c). The HAADF-STEM image (Figure 1e) and the SEM image (Figure 1f) confirm that the internal structure of the obtained Au NCPs is hollow, and a number of boundary and stacking defects can be observed on their surfaces, the existence of which is essentially necessary for the topological constraints on the spherical surface [20,24]. Additionally, Figure 1f shows the UV-Vis absorption spectra of both Au NPs and Au NCPs. The red Au NPs dispersed in water (inset of Figure 1f) exhibit a characteristic LSPR peak centered at 530 nm. In contrast, the Au NCPs (black dashed line in Figure 1f) do not display a peak at 530 nm; instead, they show a broad near-infrared plasmon absorption band, which is attributed to the strong plasmonic coupling between the Au NPs in the Au capsule shell [25]. As a result, the obtained Au NCPs are dark black in color and exhibit enhanced absorption capacity for visible light.

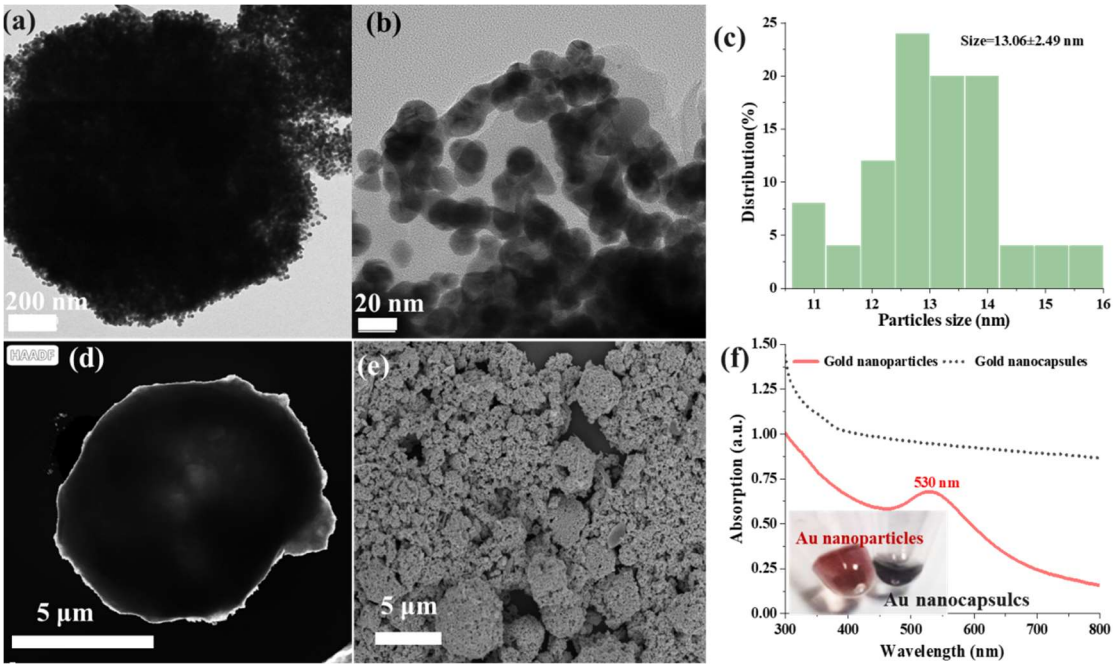

Figure 1. (**a**) Transmission electron microscopy (TEM) images of gold nanocapsules (Au NCPs); (**b**) TEM images of gold nanoparticles (Au NPs) assembled into Au NCPs; (**c**) Particle size distribution of Au NPs; (**d**) HAADF-STEM images of Au NCPs; (**e**) Scanning electron micrographs (SEM) of Au NCPs; (**f**) UV-vis absorption spectra of Au NCPs and Au NPs, the inset is a physical image of Au NPs and Au NCPs.

3.2. Photocatalytic Regeneration of NADH Performance of Au NCPs

The reduced coenzyme NADH serves as a critical cofactor for formate dehydrogenase (FDH) in catalyzing the CO_2 reduction reaction [12,26]. Previous studies have demonstrated that NADH is highly unstable and readily loses its biological activity when exposed to light [22]. Consequently, we first examined the protective properties of the electron donor triethanolamine (TEOA) and Au NCPs against NADH degradation under light exposure. As illustrated in Figure 2a, the concentration of NADH exhibited a marked decline of 78.6% following exposure to 50 mW/cm^2 white light for a period of four hours. In contrast, the concentration of NADH decreased by only 52.70% upon the addition of TEOA and illumination for the same duration. The increased stability of NADH in the TEOA system can be attributed to the alkaline nature of the TEOA and the higher stability of NADH molecules in alkaline environments [22,27]. Moreover, the concentration of NADH in the light system containing both TEOA and Au NCPs decreased by only 16.33% under identical conditions. This result indicates that NADH exhibits greater stability in the light system with Au NCPs. This enhanced stability is likely due to the excellent full-spectrum absorption properties of the Au NCPs, which effectively shield some of the photons from exerting detrimental effects on NADH molecules. Therefore, it can be concluded that the combined effect of TEOA and Au NCPs prolongs the stabilization of NADH under light illumination.

Then, using TEOA as an electron donor, we examined the performance of temperature on the photocatalytic regeneration of NADH by Au NCPs. As shown in Figure 2b, the photocatalytic regeneration yield of NADH by Au NCPs initially increased and then decreased with rising temperature. The highest regeneration yield of NADH was observed at a reaction temperature of 30 °C, where the NADH regeneration rate reached 10.10%. Since we did not add exogenous electron mediators, such as $[Cp^*Rh(bpy)H_2O]^{2+}$, which is widely used in photocatalytic coenzyme regeneration systems, the Au NCPs regenerated NADH by directly transferring photoelectrons, which resulted in a low regeneration yield of Au NCPs photocatalytic NADH, compared with other photocatalytic systems that relied on the electron mediators to transfer of photoelectrons (regeneration yield = 40~100%) [23,28,29]. This is because the yield of direct photoelectron transfer to regenerate NADH in photocatalytic systems without exogenous electron mediators (regeneration yield = 18.09~22.5%) was generally low according to previous studies [22,28]. However, considering the toxicity of organic electron donors to formate dehydrogenase [16,17], this direct electron transfer photoreaction system for regenerating coenzymes is more compatible with the FDH enzyme-catalyzed reaction.

We further optimized the light intensity and electron donor concentration for the NADH regeneration reaction. As shown in Figure 2c, under light-avoidance conditions (light intensity of 0 mW/cm²), the Au NCPs showed no regenerative activity toward NADH. The yield of NADH regeneration through Au NCPs photocatalysis initially increased and then decreased as the light intensity increased. The highest NADH regeneration yield was achieved at a light intensity of 150 mW/cm², reaching 13.56%. In addition, with the increase of TEOA concentration from 100 mM to 300 mM, the reaction equilibrium time of Au NCPs photocatalytic regeneration of NADH was shortened from 2 h to 0.5 h, and the regeneration yield of NADH was increased to 22.65% (Figure 2d). Therefore, the optimal reaction conditions for the photocatalytic regeneration of NADH by Au NCPs were temperature 30 °C, light intensity 150 mW/cm^2, and TEOA concentration 300 mM.

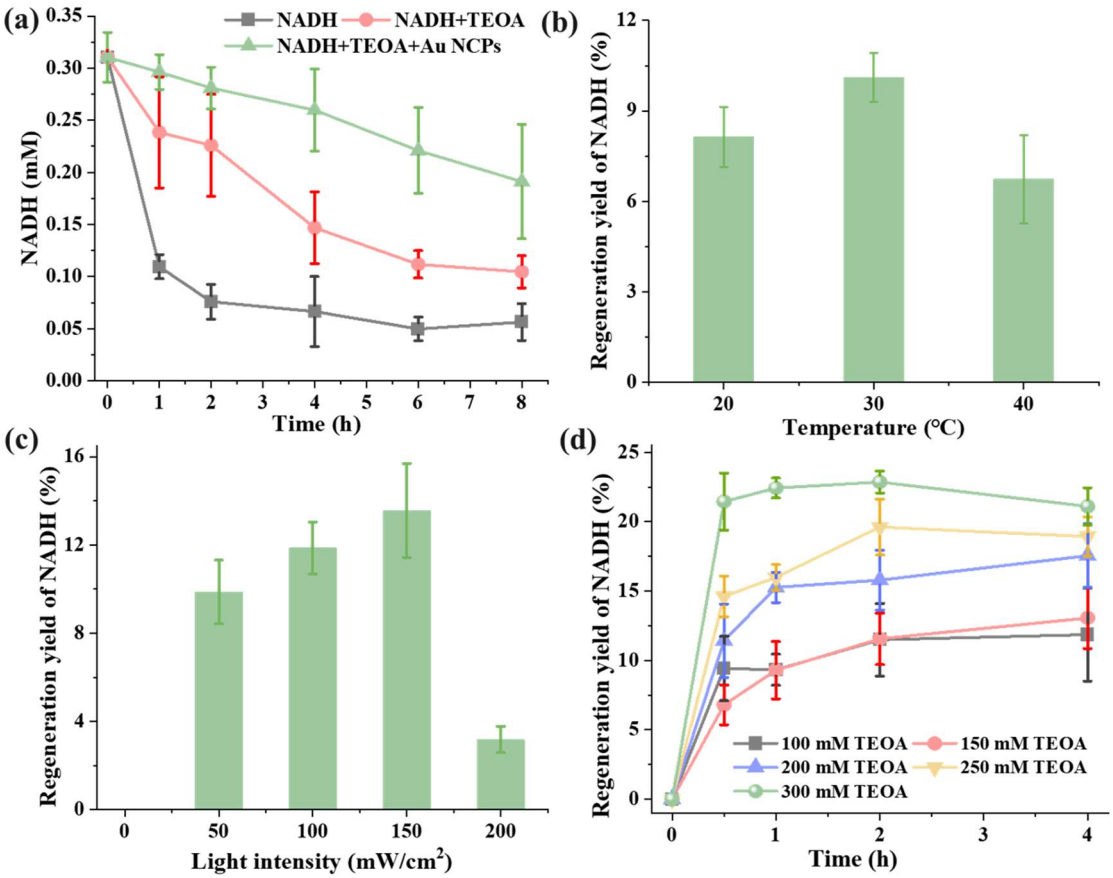

Figure 2. (**a**) Concentration change curve of NADH under white light illumination; (**b**) Regeneration yield of photocatalytic NADH by Au NCPs at different temperatures (Au NCPs: 1.25 mg/mL, TEOA: 100 mM, light intensity: 50 mW/cm^2, reaction time: four hours); (**c**) Regeneration yield of photocatalytic NADH by Au NCPs under different light intensities (Au NCPs: 1.25 mg/mL, TEOA: 100 mM, 30 °C, reaction time: four hours); (**d**) Photocatalytic NADH regeneration yield of Au NCPs at different electron donor (TEOA) concentrations (Au NCPs: 1.25 mg/mL, light intensity: 150 mW/cm^2, 30 °C).

3.3. Conformational Characterization of Au NCPs-Immobilized Formate Dehydrogenase

Furthermore, a scanning electron microscope (SEM) was used to characterize the morphology of the formate dehydrogenase (FDH) hybrids immobilized on Au NCPs. The morphology of the Au NCPs of immobilized FDH did not undergo any notable alterations (Figure 3a). Energy-dispersive X-ray (EDX) mapping scans revealed a uniform distribution of gold (Au) and molybdenum (Mo) elements in the hybrids (Figure 3b,c), with the relative mass ratio of Au at 66.34 wt% and Mo at 1.26 wt% (Figure 3d). Given that the FDH molecule contains a Mo ion active center, as previously reported in references [30,31], the uniform distribution of Mo provides strong evidence that the Au NCPs have successfully loaded FDH.

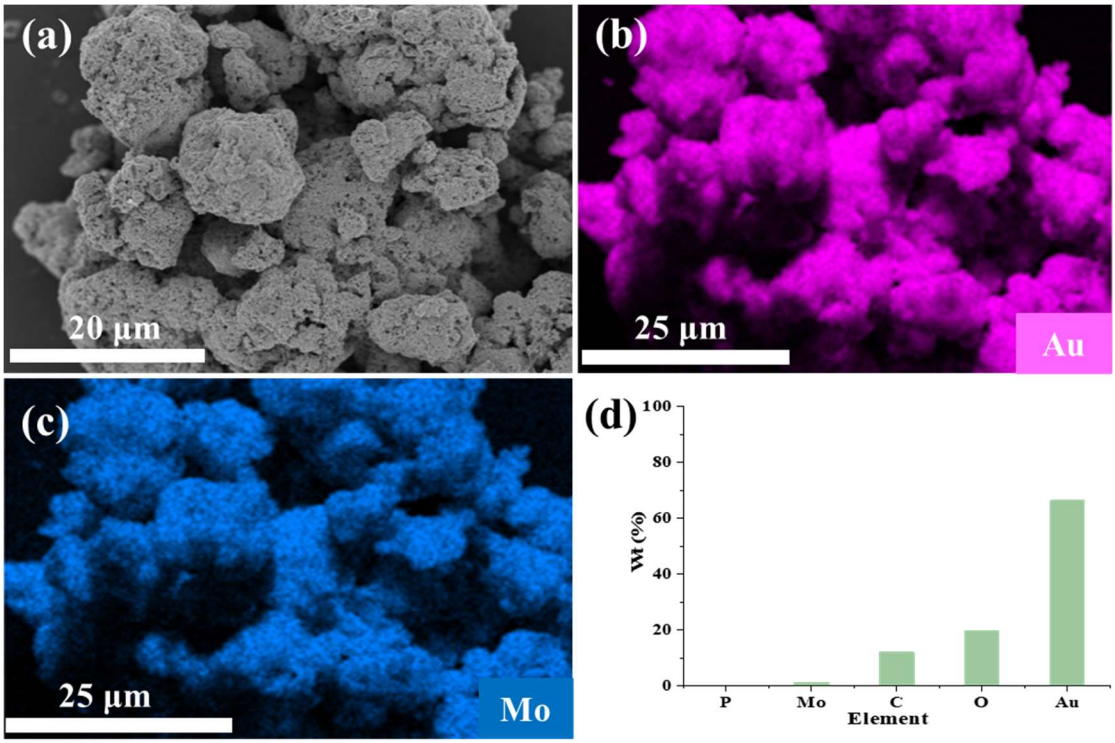

Figure 3. (**a**) SEM image of the Au NCPs hybrid with formate dehydrogenase (FDH) immobilized; the EDX mapping of gold (**b**) and molybdenum (**c**) in the Au NCPs hybrid with FDH immobilized; (**d**) the relative mass content of various elements on the surface of the hybrids.

3.4. Optimization of Conditions for the Immobilization of FDH by the Au NCPs

Since buffer composition is a critical factor influencing enzyme stability and activity [32], we investigated the amount of formate dehydrogenase (FDH) immobilized by Au NCPs in two different buffer systems: Tris-HCl and PBS. as well as the enzyme activity recovery of the immobilized FDH. As illustrated in Figure 4a, the immobilization yield of FDH by Au NCPs in both Tris-HCl and PBS buffer systems was similar; however, the enzyme activity recovery of the immobilized FDH in the PBS system was 14.35% higher than that observed in the Tris-HCl system. This finding suggests that PBS may provide a more favorable microenvironment for enzyme activity, likely due to its composition, which minimizes electrostatic interactions that could destabilize the enzyme structure. The positively charged Tris molecules may interfere with the negatively charged enzyme, reducing its bioactivity [33,34].

After establishing PBS as the preferred buffer, we further investigated the effect of reaction time on the FDH immobilization. As shown in Figure 4b, the immobilization of FDH by the Au NCPs reached equilibrium after 2 h; the FDH immobilization yield was 72.74% at this time. Subsequently, we optimized the reaction temperature within the enzyme immobilization system. The immobilization yield of FDH by the Au NCPs and the enzyme activity recovery of the immobilized FDH initially increased and then decreased with rising reaction temperature. The highest immobilization rate of FDH (73.39%) and enzyme activity recovery (74.57%) were observed at a reaction temperature of 20 °C (Figure 4c). However, at a reaction temperature of 30 °C, the enzyme activity recovery of the immobilized FDH decreased by only 3.77% compared to the 20 °C system. This indicates that the immobilized FDH maintained high enzyme activity at 30 °C, suggesting that the catalytic temperature of the immobilized FDH is well-suited for compatibility with the NADH regeneration system.

Molybdenum is a key component of the active sites of enzymes that catalyze essential redox reactions in carbon, nitrogen, and sulfur metabolism. Molybdenum ions are crucial for maintaining the stability and catalytic activity of FDH [35,36]. We further investigated the effect of sodium molybdate on the immobilization of FDH by the Au NCPs and the enzyme activity recovery of the immobilized FDH, as shown in Figure 4d, both the immobilization yield and enzyme activity recovery of FDH initially increased and then decreased with increasing sodium molybdate concentration. When the concentration of sodium molybdate was 1 mM, the highest immobilization yield and enzyme activity recovery of the immobilized FDH were achieved by the Au NCPs, which were 77.19% and 80.16%, respectively. Whereas, when the sodium molybdate concentration was increased to 2 mM, the immobilization yield and enzyme activity recovery of FDH decreased by 37.29% and 29.06%, respectively. Therefore, the optimal conditions for FDH immobilization in Au NCPs were determined to be 2 h using PBS as the buffer, a controlled temperature of 20 °C, and 1 mM sodium molybdate as a stabilizer.

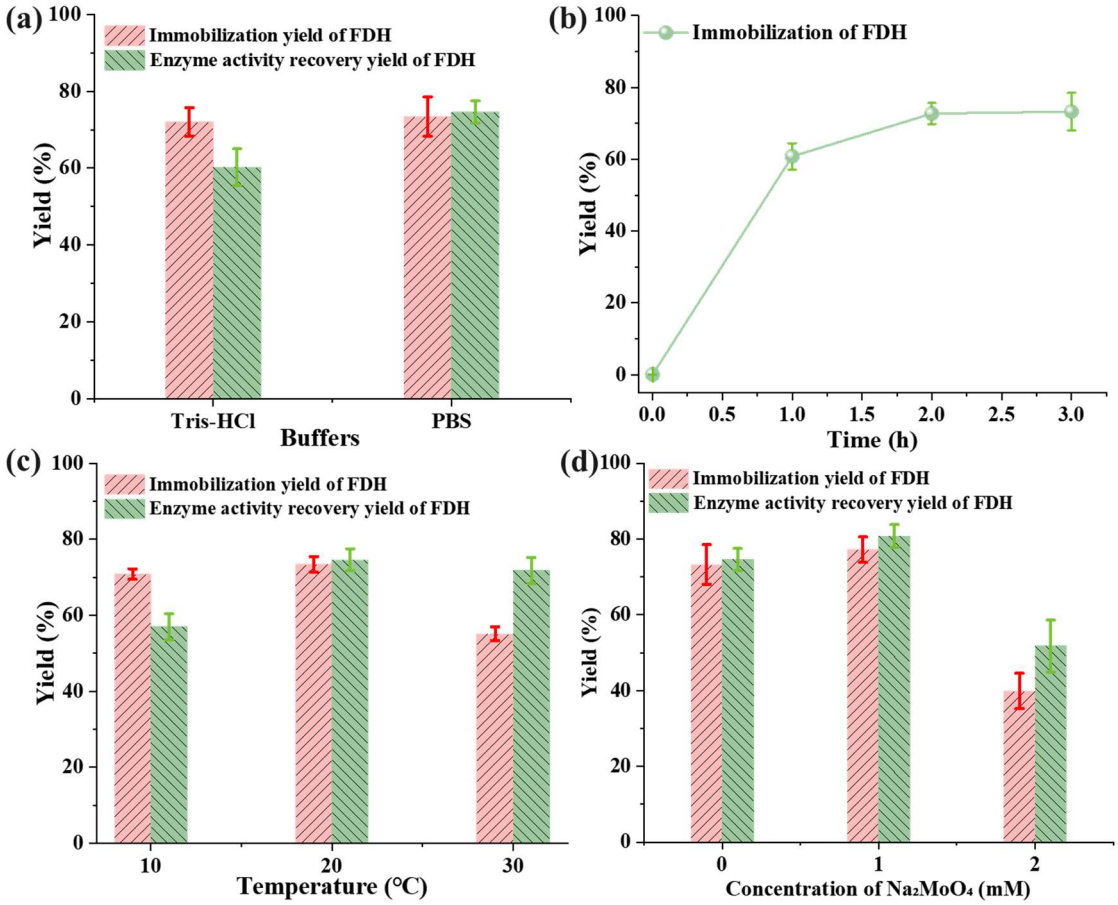

Figure 4. (**a**) Effect of immobilization of FDH by buffer (buffer: pH = 7.40, 100 mM; Au NCPs: 1.50 mg/mL; FDH: 0.10 mg/mL; 20 °C; reaction time: 2 h); (**b**) The immobilization yield of FDH by Au NCPs as a function of reaction time (pH = 7.40, 100 mM PBS; Au NCPs: 1.50 mg/mL; FDH: 0.10 mg/mL; 20 °C); (**c**) The effect of temperature on the immobilization of FDH (pH = 7.40, 100 mM PBS; Au NCPs: 1.50 mg/mL; FDH: 0.10 mg/mL; reaction time: 2 h); (**d**) The effect of sodium molybdate on the immobilization of FDH (pH = 7.40, 100 mM PBS; Au NCPs: 1.50 mg/mL; FDH: 0.10 mg/mL; 20 °C; reaction time: 2 h).

3.5. Photocatalytic CO_2 Reduction with Au NCPs-FDH Hybrids

The entry of CO_2 into solution is the primary rate-limiting step in enzyme-catalyzed carbon fixation processes [37], and considering that the formation of CO_3^{2-} from CO_2 in water is thermodynamically spontaneous ($CO_2 \rightarrow CO_3^{2-}(aq)$), with a standard Gibbs free-energy ($\Delta_f G^\theta$) of −527.8 kJ/mol [38]. Previous studies have indicated that the Na_2CO_3 can effectively absorb CO_2 [39,40]. Therefore, we investigated the impact of varying Na_2CO_3 concentrations while introducing CO_2 (99.99%) into the reaction system to assess the formate concentration produced by the Au NCPs-FDH hybrid system under illuminated conditions. As illustrated in Figure 5a, the reduction of CO_2 by the Au NCPs-FDH hybrid system in the absence of Na_2CO_3 yielded only 4.27 mg/L of formate. However, increasing the concentration of Na_2CO_3 initially resulted in an increase in formate concentration, reaching a maximum of 1.13 mM Na_2CO_3, at which point the formate concentration was twice that of the system with 0 mM Na_2CO_3. This indicates that Na_2CO_3 enhances

the reduction of CO_2 in the hybrid system, likely due to its capacity to absorb CO_2 and promote its dissolution in the liquid phase [39]. Conversely, further increases in Na_2CO_3 concentration resulted in a rapid decline in formate levels to approximately 4 mg/L, comparable to the 0 mM Na_2CO_3 condition. This decrease may be attributed to a reduction in the bulk mass transfer coefficient of the solution at high Na_2CO_3 concentrations, which significantly lowers the CO_2 diffusion coefficient [39], thereby resulting in reduced formate production.

We further investigated the performance of free FDH and the Au NCPs-FDH hybrid system in reducing CO_2 to produce formate under light exposure. The Au NCPs-FDH hybrid system demonstrated a higher formate synthesis rate (1.39 mg/L/h) compared to free FDH (0.84 mg/L/h). After 8 h of light exposure, the cumulative formate concentration in the Au NCPs-FDH hybrid system was 1.65 times greater than that of the free FDH system (Figure 5b). These results indicate that the Au NCPs-FDH hybrid system effectively facilitates the light-driven reduction of CO_2 to formate.

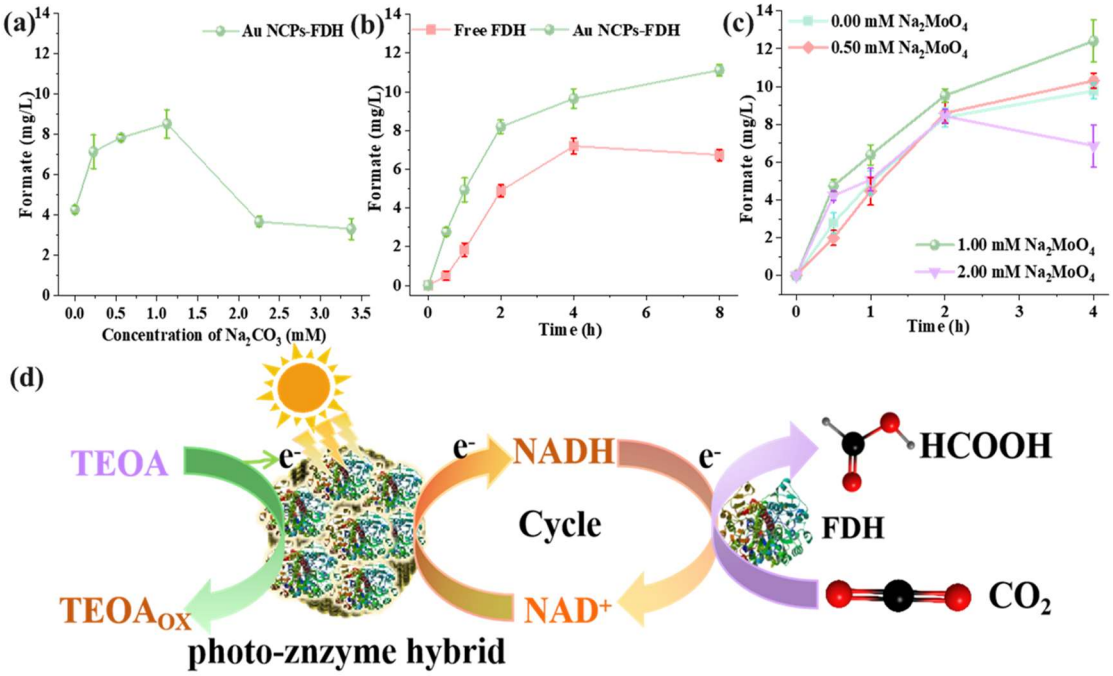

Figure 5. (**a**) Effect of sodium carbonate on the photocatalytic reduction of CO_2 to formate by Au NCPs-FDH hybrid (reaction time: 2 h); (**b**) Comparison of the performance of immobilized enzyme and free enzyme in reducing CO_2 under light (Na_2CO_3: 1.10 mM); (**c**) Effect of sodium molybdate on the photocatalytic reduction of CO_2 to formate by Au NCPs-FDH hybrid; (**d**) Schematic diagram of the mechanism for the continuous conversion of CO_2 to formate by Au NCPs-FDH hybrid system under Visible Light.

Furthermore, the addition of the FDH stabilizer sodium molybdate to the Au NCPs-FDH hybrid system, as illustrated in Figure 5c, revealed that as the sodium molybdate concentration increased, the formate concentration of the hybrid system exhibited a pattern of initial increase and subsequent decrease. At a sodium molybdate concentration of 1 mM, the hybrid system achieved the highest formate concentration after 4 h of light exposure, reaching a concentration of 12.41 mg/L (269.61 μM). Additionally, the operation of the photo-enzyme hybrid system is illustrated in Figure 5d. The Au NCPs act as a light absorber and charge generator. The photo-excited electrons generated by the Au NCPs directly reduce NAD^+ in situ to produce NADH, which then serves as a coenzyme for FDH, driving the conversion of CO_2 to formate. The released NAD^+ is further reduced by photoelectrons from the Au NCPs, enabling the cyclic regeneration of NADH. . Simultaneously, TEOA light oxidation replenishes the electrons consumed in the regeneration of NADH by the Au NCPs.

Moreover, the rate of formate production from CO_2 using the Au NCPs-FDH hybrid system under light exposure was compared with findings from other studies. The current system, which does not employ organic electron mediators, achieved a formate production rate of 67.40 μM/L/h with TEOA as the electron donor over 4 h of light exposure, obviously higher than most of the reported values (Table 1). This further demonstrates the efficiency and rapidity of the Au NCPs—FDH hybrid system in converting CO_2 to formate.

Table 1. Comparison of the performance of the photo-enzymatic conversion of CO_2 to formate.

Enzyme	Light	Electron Donor	Electron Mediator	Formate Production Rate (μM/L/h)	Ref.
Free FDH	λ ≥ 420 nm	TEOA (300 mM)	Cp*Rh(bpy)Cl (500 mM)	2.61	[26]
10%In-CdS@ZIF-8&FDH	λ ≥ 420 nm	TEOA (300 mM)	Cp*Rh(bpy)Cl (500 mM)	11.13	[26]
FDH@ZIF-8/g-C_3N_4	λ ≥ 420 nm	TEOA (670 mM)	$[Cp^*Rh(bpy)(H_2O)]^{2+}$ (3.90 mM)	15.00	[37]
CA&FDH@ZIF-8/g-C_3N_4	λ ≥ 420 nm	TEOA (670 mM)	$[Cp^*Rh(bpy)(H_2O)]^{2+}$ (3.90 mM)	48.60	[37]
UV/TiO_2@FDH	Λ = 365 nm	EDTA (0.25 mM)	$[Cp^*Rh(bpy)(H_2O)]^{2+}$ (0.22 mM)	255.56	[3]
Eosin Y/cobaloxime@FDH	λ ≥ 420 nm	TEOA (200 mM)	No	35.00	[41]
GO-Co-ATPP@FDH	λ ≥ 420 nm	TEOA (413 mM)	methyl viologen (0.21 mM)	48.25	[42]
TCPP/SiO_2/Rh HNPs@FDH	λ ≥ 420 nm	TEOA (1000 mM)	Cp*Rh(bpy)Cl (0.15 mM)	20.00	[15]
CCGCMAQSP@FDH	λ ≥ 420 nm	TEOA (400 mM)	Cp*Rh(bpy)Cl (0.20 mM)	55.28	[43]
5%Ti_3C_2/C_3N_5@FDH	λ ≥ 420 nm, 100 mW/cm^2	TEOA (1000 mM)	No	33.33	[13]
Au NCPs—FDH	λ ≥ 400 nm, 150 mW/cm^2	TEOA (300 mM)	No	67.40	This work

4. Conclusions

In conclusion, the photo-enzymatic hybrid system developed in this study, which integrates gold nanocapsule photocatalysts with formate dehydrogenase (FDH), successfully facilitated the light-driven in situ regeneration of NADH coenzymes for highly efficient catalytic CO_2 reduction to produce formate. The reaction was conducted under irradiation with 150 mW/cm^2 of white light, utilizing 300 mM TEOA as the electron donor, 1.10 mM Na_2CO_3 as a CO_2 absorbent (supplemental carbon source), and 1 mM sodium molybdate as a stabilizer for FDH. Notably, this photo-enzymatic hybrid system achieved the highest formate concentration and production rate observed in this context, with a production rate that was 3.68 times greater than that of the free FDH-catalyzed system. This work demonstrates the feasibility of employing photo-enzymatic coupling for the continuous synthesis of formate from CO_2, highlighting the potential for sustainable CO_2 conversion technologies.

Author Contributions

Conceptualization, G.X. and H.S.; Methodology, Y.W.; Software, Y.W.; Validation, Y.W., M.G. and H.W.; Formal Analysis, Y.W.; Investigation, Y.W., M.G. and H.W.; Resources, J.X.; Data Curation, Y.W.; Writing—Original Draft Preparation, Y.W.; Writing—Review & Editing, G.X. and H.S.; Visualization, Y.W.; Supervision, H.S.; Project Administration, Y.W.; Funding Acquisition, G.X. and H.S.

Ethics Statement

Not applicable.

Informed Consent Statement

Not applicable.

Funding

This research was funded by the National Key R&D Program of China (Grant Nos. 2021YFC2103600) and the National Natural Science Foundation of China (Grant Nos. 22408378 and 22408019).

Declaration of Competing Interest

The authors declare that they have no known competing financial interests or personal relationships that could have appeared to influence the work reported in this paper.

References

1. Liu G, Wang L, Yan L, Zhao H, Li Y, Zhou L, et al. A dual-enzyme microreactor based on encapsulation and covalent bond for enzymatic electrocatalytic CO_2 reduction. *Chem. Eng. J.* **2023**, *475*, 146186.
2. Chai SYW, Ngu LH, How BS. Review of carbon capture absorbents for CO_2 utilization. *Greenh. Gases Sci. Technol.* **2022**, *12*, 394–427.
3. Gu F, Wang Y, Meng Z, Liu W, Qiu L. A coupled photocatalytic/enzymatic system for sustainable conversion of CO_2 to formate. *Catal. Commun.* **2020**, *136*, 105903.
4. Moon M, Park GW, Lee J-p, Lee J-S, Min K. Recent progress in formate dehydrogenase (FDH) as a non-photosynthetic CO_2 utilizing enzyme: A short review. *J. CO_2 Util.* **2020**, *42*, 101353.
5. Liu W, Hou Y, Hou B, Zhao Z. Enzyme-catalyzed sequential reduction of carbon dioxide to formaldehyde. *Chin. J. Chem. Eng.* **2014**, *22*, 1328–1332.
6. Ji X, Su Z, Wang P, Ma G, Zhang S. Tethering of nicotinamide adenine dinucleotide inside hollow nanofibers for high-yield synthesis of methanol from carbon dioxide catalyzed by coencapsulated multienzymes. *Acs Nano* **2015**, *9*, 4600–4610.
7. Zhu D, Ao S, Deng H, Wang M, Qin C, Zhang J, et al. Ordered coimmobilization of a multienzyme cascade system with a metal organic framework in a membrane: Reduction of CO_2 to methanol. *ACS Appl. Mater. Interfaces* **2019**, *11*, 33581–33588.
8. Ryu J, Lee SH, Nam DH, Park CB. Rational Design and Engineering of Quantum-Dot-Sensitized TiO_2 Nanotube Arrays for Artificial Photosynthesis. *Adv. Mater.* **2011**, *16*, 1883–1888.
9. Ji X, Su Z, Wang P, Ma G, Zhang S. Integration of artificial photosynthesis system for enhanced electronic energy-transfer efficacy: A case study for solar-energy driven bioconversion of carbon dioxide to methanol. *Small* **2016**, *12*, 4753–4762.
10. Huang X, Wang B, Wang Y, Jiang G, Feng J, Zhao H. Photoenzymatic enantioselective intermolecular radical hydroalkylation. *Nature* **2020**, *584*, 69–74.
11. Hutton GA, Reuillard B, Martindale BC, Caputo CA, Lockwood CW, Butt JN, et al. Carbon dots as versatile photosensitizers for solar-driven catalysis with redox enzymes. *J. Am. Chem. Soc.* **2016**, *138*, 16722–16730.
12. Guo M, Gu F, Meng L, Liao Q, Meng Z, Liu W. Synthesis of formaldehyde from CO_2 catalyzed by the coupled photo-enzyme system. *Sep. Purif. Technol.* **2022**, *286*, 120480.
13. Yang F, Zhang P, Qu J, Yang X, Cai Y, Li CM, et al. Highly efficient photoenzymatic CO_2 reduction dominated by 2D/2D MXene/C_3N_5 heterostructured artificial photosynthesis platform. *J. Colloid Interface Sci.* **2025**, *678*, 1121–1131.
14. Tan Y, Ma J, Zhang F, Wang S, Lan F, Liu H, et al. Polymer Photocatalyst–Enzyme Coupled Artificial Photosynthesis System for CO_2 Reduction into Formate Using Water as the Electron Donor. *ACS Sustain. Chem. Eng.* **2022**, *10*, 12065–12071.
15. Ji X, Wang J, Mei L, Tao W, Barrett A, Su Z, et al. Porphyrin/SiO_2/Cp*Rh(bpy)Cl Hybrid nanoparticles mimicking chloroplast with enhanced electronic energy transfer for biocatalyzed artificial photosynthesis. *Adv. Funct. Mater.* **2018**, *28*, 1705083.
16. Himiyama T, Waki M, Maegawa Y, Inagaki S. Cooperative catalysis of an alcohol dehydrogenase and rhodium-modified periodic mesoporous organosilica. *Angew. Chem.* **2019**, *131*, 9248–9252.
17. Zhang P, Dong W, Zhang Y, Zhao L-N, Yuan H, Wang C, et al. Metalated carbon nitride with facilitated electron transfer pathway for selective NADH regeneration and photoenzyme-coupled CO_2 reduction. *Chin. J. Catal.* **2023**, *54*, 188–198.
18. Lian X, Fang Y, Joseph E, Wang Q, Li J, Banerjee S, et al. Enzyme–MOF (metal–organic framework) composites. *Chem. Soc. Rev.* **2017**, *46*, 3386–3401.
19. Zhang L, Can M, Ragsdale SW, Armstrong FA. Fast and selective photoreduction of CO_2 to CO catalyzed by a complex of carbon monoxide dehydrogenase, TiO_2, and Ag nanoclusters. *ACS catal.* **2018**, *8*, 2789–2795.
20. Liu D, Zhou F, Li C, Zhang T, Zhang H, Cai W, et al. Black Gold: Plasmonic Colloidosomes with Broadband Absorption Self-Assembled from Monodispersed Gold Nanospheres by Using a Reverse Emulsion System. *Angew. Chem. Int. Ed.* **2015**, *54*, 9596–9600.
21. Li X, Sun H, Mao X, Lao Y, Chen F. Enhanced photosynthesis of carotenoids in microalgae driven by light-harvesting gold nanoparticles. *ACS Sustain. Chem. Eng.* **2020**, *8*, 7600–7608.
22. Wang Y, Jin Y, Wang Z, Xiao G, Su H. A Light-Dark Cascade Procedure for the Regeneration of NADH using Graphitic Carbon Nitride Nanosheets. *ChemPhotoChem* **2022**, *6*, e202200067.
23. Wu Y, Ward-Bond J, Li D, Zhang S, Shi J, Jiang Z. g-C_3N_4@ α-Fe_2O_3/C photocatalysts: Synergistically intensified charge generation and charge transfer for NADH regeneration. *ACS Catal.* **2018**, *8*, 5664–5674.
24. Xu X-W, Zhang X-M, Liu C, Yang Y-L, Liu J-W, Cong H-P, et al. One-pot colloidal chemistry route to homogeneous and doped colloidosomes. *J. Am. Chem. Soc.* **2013**, *135*, 12928–12931.
25. Song J, Cheng L, Liu A, Yin J, Kuang M, Duan H. Plasmonic vesicles of amphiphilic gold nanocrystals: Self-assembly and external-stimuli-triggered destruction. *J. Am. Chem. Soc.* **2011**, *133*, 10760–10763.

26. Zhou J, Tian X, Yu S, Zhao Z, Ji Y, Schwanebrg U, et al. In-CdS@ ZIF-8&FDH photo-enzyme nanosystem with high NADH regeneration ability via indium doping for enhanced CO_2 reduction to formic acid. *Chem. Eng. Sci.* **2024**, *285*, 119613.
27. Wong C-H, Whitesides GM. Enzyme-catalyzed organic synthesis: NAD(P)H cofactor regeneration by using glucose-6-phosphate and the glucose-5-phosphate dehydrogenase from Leuconostoc mesenteroides. *J. Am. Chem. Soc.* **1981**, *103*, 4890–4899.
28. Fang W, Deng Y, Tang L, Zeng G, Zhou Y, Xie X, et al. Synthesis of Pd/Au bimetallic nanoparticle-loaded ultrathin graphitic carbon nitride nanosheets for highly efficient catalytic reduction of p-nitrophenol. *J. Colloid Interface Sci.* **2017**, *490*, 834–843.
29. Huang J, Antonietti M, Liu J. Bio-inspired carbon nitride mesoporous spheres for artificial photosynthesis: Photocatalytic cofactor regeneration for sustainable enzymatic synthesis. *J. Mater. Chem. A* **2014**, *2*, 7686–7693.
30. Cordas CM, Campaniço M, Baptista R, Maia LB, Moura I, Moura JJ. Direct electrochemical reduction of carbon dioxide by a molybdenum-containing formate dehydrogenase. *J. Inorg. Biochem.* **2019**, *196*, 110694.
31. Dong G, Ryde U. Reaction mechanism of formate dehydrogenase studied by computational methods. *JBIC J. Biol. Inorg. Chem.* **2018**, *23*, 1243–1254.
32. Wei T, Kaewtathip S, Shing K. Buffer effect on protein adsorption at liquid/solid interface. *J. Phys. Chem. C* **2009**, *113*, 2053–2062.
33. Sigurdardóttir SB, Lehmann J, Grivel JC, Zhang W, Kaiser A, Pinelo M. Alcohol dehydrogenase on inorganic powders: Zeta potential and particle agglomeration as main factors determining activity during immobilization. *Colloids Surf. B* **2019**, *175*, 136–142.
34. Cugia F, Monduzzi M, Ninham BW, Salis A. Interplay of ion specificity, pH and buffers: Insights from electrophoretic mobility and pH measurements of lysozyme solutions. *RSC Adv.* **2013**, *3*, 5882–5888.
35. Bulut H, Valjakka J, Yuksel B, Yilmazer B, Turunen O, Binay B. Effect of metal ions on the activity of ten NAD-dependent formate dehydrogenases. *Protein J.* **2020**, *39*, 519–530.
36. Maia LB, Moura JJ, Moura I. Molybdenum and tungsten-dependent formate dehydrogenases. *BIC J. Biol. Inorg. Chem.* **2015**, *20*, 287–309.
37. Yu S, Lv P, Xue P, Wang K, Yang Q, Zhou J, et al. Light-driven enzymatic nanosystem for highly selective production of formic acid from CO_2. *Chem. Eng. J.* **2021**, *420*, 127649.
38. Zheng Y, Zhang W, Li Y, Chen J, Yu B, Wang J, et al. Energy related CO_2 conversion and utilization: Advanced materials/nanomaterials, reaction mechanisms and technologies. *Nano Energy* **2017**, *40*, 512–539.
39. Fang C, Zhang H, Xiao Y, Zhao T, Zou R, Luo G, et al. Carbon dioxide capture in sodium carbonate solution: Mass transfer kinetics and DTAC surfactant enhancement mechanism. *Carbon Capture Sci. Technol.* **2024**, *13*, 100270.
40. Park SW, Sung DH, Choi BS, Oh KJ, Moon KH. Sorption of carbon dioxide onto sodium carbonate. *Sep. Sci. Technol.* **2006**, *41*, 2665–2684.
41. Kim JA, Kim S, Lee J, Baeg J-O, Kim J. Photochemical production of NADH using cobaloxime catalysts and visible-light energy. *Inorg. Chem.* **2012**, *51*, 8057–8063.
42. Kumar S, Yadav RK, Ram K, Aguiar A, Koh J, Sobral AJ. Graphene oxide modified cobalt metallated porphyrin photocatalyst for conversion of formic acid from carbon dioxide. *J. CO_2 Util.* **2018**, *27*, 107–114.
43. Yadav RK, Baeg J-O, Oh GH, Park N-J, Kong K-j, Kim J, et al. A photocatalyst–enzyme coupled artificial photosynthesis system for solar energy in production of formic acid from CO_2. *J. Am. Chem. Soc.* **2012**, *134*, 11455–11461.